Conductive response of a photo-excited sample in a radio-frequent driven resonance cavity

Juleon M. Schins and Elise Talgorn
Opto-Electronic Materials Section, Department of Chemical Engineering, Delft University of Technology, Julianalaan 136, 2628 BL Delft, The Netherlands

(Received 23 March 2011; accepted 19 May 2011; published online 16 June 2011)

An expression is derived for the perturbative response of a lumped resonance circuit to a sudden change in the circuit parameters. This expression is shown to describe also the photo-induced conductivity of a semiconductor mounted in a single-mode microwave cavity. The power dissipated in the cavity is measured in the two dimensions corresponding to time (after photo-excitation of the sample) and frequency (of the microwave driving source). Analysis of the experimental data for different semiconductor materials demonstrates the general applicability of the presented analytical expression here, by retrieving the time dependence of the sample's photo-induced conductivity. © *2011 American Institute of Physics*. [doi:10.1063/1.3600062]

I. HISTORICAL INTRODUCTION

In 1946 Margenau calculated the complex conductivity as a function of gas pressure and frequency of the driving field.[1] His expression interpolated existing expressions at two limits. In the limit of high frequency and low pressure the current induced in the ionized gas is in quadrature with the driving field: due to the inertia of free electrons their acceleration is in phase with the field, and their velocity (or current) lags the field by 90°. On the other hand, and at low frequency and high pressure the current is in phase with the driving field, as described by Langevin's mobility formula. In frequency space the current J is linearly related to the driving field E as $J(\omega) = \sigma(\omega)E(\omega)$, with σ the complex conductivity. When the current is in phase with the driving field the conductivity is real, causing absorption of microwaves by the gas due to collisions of electrons with gas molecules; when the current is in quadrature with the driving field the conductivity is imaginary, causing dispersion of the microwaves in the gas, i.e., a change in the index of refraction with respect to vacuum.

In the same year Margenau and co-workers reported their first results on the recovery of gas-filled switching tubes.[2] These tubes made it possible to use the same antenna and transmission line for pulse radar transmission and reception. The major technological issue was the recovery of the discharge producing the radar pulse. If the same tube were to be used for the resonant detection of reflected radar pulses, the cavity should be restored to resonance as soon as possible after pulse emission. The authors achieved this goal by the use of electron-scavenging gases, such as oxygen, argon-pentene, and argon-H_2S mixtures. This work paved the way for time-resolved experiments using transients in microwave conductivity.

The first experimental setup of what today is known under the acronym TRMC, standing for time-resolved microwave conductivity, was published by Biondi and Brown in 1949.[3] This setup was initially used to perform experiments in the gas phase.[4–10] In the 1960s and 1970s, TRMC was first applied to solid-state inorganic semiconductor materials.[11–13] In 1973 the technique was first applied to the charge carrier dynamics in liquid hydrocarbons, excited by a nanosecond pulse of highly energetic (several MeV) electrons.[14] This technique has since then been used successfully for the study of several kinds of solids, such as ice,[15,16] DNA,[17–19] buckminsterfullerene,[20] columnar stacked aggregates,[21] and polymers.[22] The study of conjugate polymers was boosted with the introduction of laser pulses as an ionizing source.[23,24] TRMC is now being used routinely as a method to determine transient conductivities of a wide variety of materials, such as silicon-based composites for solar cells,[25–28] compound semiconductors,[29,30] columnar stacked molecular aggregates,[31–39] bulk solids or thin films of conjugated polymers,[40–47] and molecular wires in dilute solution.[44,48–52] The technique proves particularly useful for measuring charge separation, e.g., electron injection from a photo-excited dye molecule into nanocrystalline TiO_2,[53–55] from a CdS coating into mesoporous TiO_2 and ZrO_2,[56] from P3HT into ZnMgO,[57] and into PCBM, a Fullerene derivative of the C_{60} Buckyball.[58,59]

The TRMC principle is based on the microwave reflectivity measurement of a resonant cavity containing the sample. When the sample is not excited, most of the microwaves are reflected from the resonant cavity, except at resonance. Due to the high quality factor of the resonant cavity, at resonance a large part of the incident microwave power is absorbed, even if the sample is hardly conductive. Due to excitation of the sample with a nanosecond laser pulse, or a MeV electron pulse, the sample exhibits transient conductivity. This conductivity changes the dielectric properties of the resonant cavity, which in turn changes the amount of reflected microwave power. From the measurement of the reflected microwave power it is possible to infer the two components of the frequency-dependent complex conductivity: the real component describes the change in absorption, and the imaginary component describes the change in dielectric constant.

There have been attempts to provide a theoretical framework taking into account the time dependence of the conductivity, triggered by the temporal behavior of samples with an imaginary component of the conductivity.[60–62] However, a

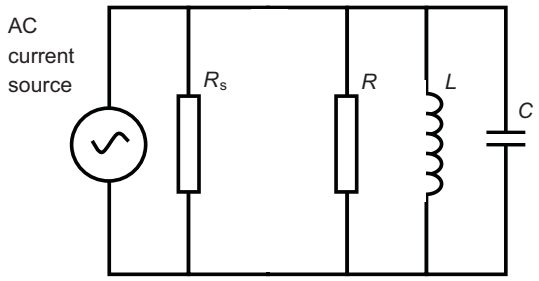

FIG. 1. Resonant RLC circuit driven by a current source with source impedance R_S.

complete and consistent time-dependent description has not yet been published to the best of our knowledge. Here, we present the theory of a lumped element circuit containing time-dependent elements. The theory will be validated with data from TRMC measurements.

II. RLC CIRCUIT WITH TIME-INDEPENDENT PARAMETER VALUES

A lumped element circuit is shown in Fig. 1. The symbols R, L, and C represent a resistor, inductor, and capacitor, respectively. The current source has an internal or source resistance, R_S. For a sinusoidal driving current $I_0 \sin \omega t$ the voltage across the circuit is determined by

$$C\dot{V}(t) + \left(\frac{1}{R_S} + \frac{1}{R}\right) V(t) + \frac{1}{L}\int_{-\infty}^{t} dt'\ V(t') = I_0 \sin(\omega t). \tag{1}$$

The driving frequency is denoted by ω and the time by t. For time-independent values of the circuit parameters, now labeled with a sub-index (R_0, L_0, and C_0), the integral of Eq. (1) can be eliminated by taking the derivative to time

$$\ddot{V}_0(t) + (\gamma_0 + \gamma_S)\dot{V}_0(t) + K_0 V_0(t) = \frac{\omega I_0}{C_0}\cos(\omega t)$$
$$\gamma_0 = \frac{1}{R_0 C_0};\quad \gamma_S = \frac{1}{R_S C_0};\quad K_0 = \frac{1}{L_0 C_0}. \tag{2}$$

The solution to Eq. (2) reads

$$V_0(t) = \frac{\omega I_0}{C_0}\mathrm{Re}(\tilde{G}(\omega)e^{i\omega t}), \tag{3}$$

with $\tilde{G}(\omega)$ the frequency-resolved Green function

$$\tilde{G}(\omega) = \frac{1}{K_0 - \omega^2 + i\omega(\gamma_0 + \gamma_S)}. \tag{4}$$

The Green function has two poles, located in the upper half plane, at

$$\omega = i\bar{\gamma} \pm \Omega,\ \text{with}\ \Omega^2 = K_0 - \bar{\gamma}^2; \bar{\gamma} \equiv \frac{\gamma_0 + \gamma_S}{2}. \tag{5}$$

These poles will be used for the calculation of the pump-induced cycle-averaged power in the final section. The sign of Ω^2 determines the behavior of the lumped circuit: overdamped (negative Ω^2) versus underdamped (positive Ω^2). Note that in the underdamped case the oscillation frequency of the transient (Ω) is lower than the resonance frequency ($\omega_{\mathrm{res}} \equiv \sqrt{K_0}$). The steady-state cycle-averaged power $\bar{P}_0^{\mathrm{diss}}$ dissipated in the RLC circuit follows directly from Eqs. (3) and (4),

$$\begin{aligned}\bar{P}_0^{\mathrm{diss}} &\equiv \frac{1}{T}\int_0^T dt\ V_0(t)[I_R(t) + I_L(t) + I_C(t)] \\ &= \frac{1}{T}\int_0^T dt\ V_0(t)\left(I_0 \sin(\omega t) - \frac{V_0(t)}{R_S}\right) \\ &= 4\omega^2 \gamma_0 \gamma_S P_{AV} |\tilde{G}(\omega)|^2.\end{aligned} \tag{6}$$

Here, $T = 2\pi/\omega$ is the cycle period, and I_R, I_L, and I_C, are the three currents flowing through the resistance, inductance, and capacitance, respectively. P_{AV} represents the maximum available power from the source, and is given by

$$P_{AV} = \frac{I_0^2 R_S}{8}. \tag{7}$$

The dissipated power peaks at resonance $\sqrt{K_0}$ for all given values of the circuit resistances. For future reference the normalized reflected power at resonance is expressed in terms of the circuit resistances as follows:

$$\left.\frac{\bar{P}_0^{\mathrm{refl}}}{P_{AV}}\right|_{\omega_{\mathrm{res}}} \equiv 1 - \left.\frac{\bar{P}_0^{\mathrm{diss}}}{P_{AV}}\right|_{\omega_{\mathrm{res}}} = 1 - 4\frac{\gamma_0\gamma_S}{(\gamma_0 + \gamma_S)^2} = \left(\frac{\gamma_0 - \gamma_S}{\gamma_0 + \gamma_S}\right)^2. \tag{8}$$

Clearly, for $\gamma_0 = \gamma_S$ all available power from the source is dissipated in the cavity. The cavity is then said to be *critically coupled* to the waveguide. This coupling is used typically in electron spin resonance setups, in which the sensitivity is optimized for absorptive changes, and the signal is heterodyned by mixing in part of the source. However, this way of heterodyning is not capable of optimizing both absorptive and dielectric changes at the time.

Finally, the inverse quality factor of the loaded cavity is given by the ratio of the full width at half maximum (FWHM) of the dissipated power (Eq. (6)) and the resonance frequency ω_{res},

$$Q_{\mathrm{loaded}}^{-1} \equiv \frac{FWHM}{\omega_{\mathrm{res}}} = Q_{\mathrm{sample}}^{-1} + Q_{\mathrm{unloaded}}^{-1}$$
$$Q_{\mathrm{sample}}^{-1} = \frac{\gamma_0}{\omega_{\mathrm{res}}}, Q_{\mathrm{unloaded}}^{-1} = \frac{\gamma_S}{\omega_{\mathrm{res}}}. \tag{9}$$

The two terms correspond to the inverse quality factors of the sample only (γ_0) and of the unloaded cavity (γ_S); the latter can again be decomposed into a component describing the heat loss due to field-sustaining currents in the cavity walls, and a component describing field leakage through the iris: $Q_{\mathrm{unloaded}}^{-1} = Q_{\mathrm{wall}}^{-1} + Q_{\mathrm{iris}}^{-1}$. The source resistance R_S accounts for both these components, implying the relation $\gamma_S^{-1} = \gamma_{\mathrm{wall}}^{-1} + \gamma_{\mathrm{iris}}^{-1}$. In the remainder of this paper, the contributions of wall and iris will always be lumped together in the single quantity γ_S.

III. RLC CIRCUIT WITH TIME-DEPENDENT PARAMETER VALUES

For temporally varying circuit parameters the differential equation corresponding to Eq. (2) must be augmented with the temporal derivatives to those parameters,

$$\ddot{V}(t) + [\gamma_S + \gamma(t)]\dot{V}(t) + [K(t) + \dot{\gamma}(t)]V(t) + \dot{K}(t)\int_{-\infty}^{t} dt'\ V(t') = \frac{\omega I_0}{C_0}\cos(\omega t). \tag{10}$$

Here, we used the definitions

$$\gamma(t) = \frac{1}{R(t)C_0}; \quad \gamma_S = \frac{1}{R_S C_0}; \quad K(t) = \frac{1}{L(t)C_0}. \tag{11}$$

Equation (10) accounts for changes in the resistor and inductor only. It is easily generalized to inclusion of changes in the capacitor, too, but for the present purpose it is general enough. For small changes of the circuit parameters, Eq. (10) can be linearized. To this end we introduce the following differential quantities:

$$\begin{aligned} u(t) &\equiv V(t) - V_0(t) \\ \delta\gamma(t) &\equiv \gamma(t) - \gamma_0 \\ \delta K(t) &\equiv K(t) - K_0 \end{aligned} . \tag{12}$$

They satisfy the following differential equation

$$[\ddot{V}_0(t) + \ddot{u}(t)] + [\gamma_S + \gamma_0 + \delta\gamma(t)][\dot{V}_0(t) + \dot{u}(t)] + [K_0 + \delta K(t) + \delta\dot{\gamma}(t)][V_0(t) + u(t)] + \delta\dot{K}(t) \times \int_{-\infty}^{t} dt'\ [V_0(t') + u(t')] = \frac{\omega I_0}{C_0}\cos(\omega t). \tag{13}$$

The linearization is obtained by neglecting products of two differential quantities, such as, e.g., $\delta\gamma(t)\dot{u}(t)$. Next we subtract Eq. (1) from Eq. (13). A second order differential equation for the differential voltage *u(t)* results

$$\begin{aligned} &\ddot{u}(t) + [\gamma_S + \gamma_0]\dot{u}(t) + K_0 u(t) = S(t) \\ &S(t) \equiv -\dot{V}_0(t)\delta\gamma(t) - V_0(t)[\delta K(t) + \delta\dot{\gamma}(t)] \\ &\qquad - \delta\dot{K}(t)\int_{-\infty}^{t} dt' V_0(t'). \end{aligned} \tag{14}$$

The source term *S(t)* depends on the steady-state solution V_0, as well as on the differential circuit parameters $\delta\gamma(t)$, $\delta K(t)$. The solution of Eq. (14) for the differential voltage *u(t)* is a temporal convolution of the Green function of Eq. (4) with the above source term *S(t)*. In frequency space a temporal convolution becomes a simple product,

$$\begin{aligned} u(t) &= \int dt' G(t - t')S(t') \\ \tilde{u}(q) &= \tilde{G}(q)\tilde{S}(q). \end{aligned} \tag{15}$$

The functions labeled with a tilde are Fourier transforms of time-domain functions. Throughout this paper the following convention is used:

$$\begin{aligned} \tilde{f}(q) &= \int dt\ e^{-iqt} f(t) \\ f(t) &= \frac{1}{2\pi}\int dq\ e^{iqt}\tilde{f}(q). \end{aligned} \tag{16}$$

IV. SOURCE TERM

In this section, the source term $\tilde{S}(q)$ will be calculated for a single-exponential time dependence of the differential circuit parameters; and subsequently, the differential cycle-averaged power will be derived. The differential circuit parameters are given by

$$\begin{aligned} \delta\gamma(t) &= \delta\gamma_0\ \theta(t)\, e^{-\Gamma t} \\ \delta K(t) &= \delta K_0\ \theta(t)\, e^{-\Gamma t}. \end{aligned} \tag{17}$$

Here Γ represents the lifetime of the charge carrier causing the change of the circuit parameters, and *θ(t)* stands for the Heaviside function. The source term reads

$$-S(t) = [\dot{V}_0(t)\delta\gamma_0 + V_0(t)\delta K_0]\theta(t)e^{-\Gamma t} - \Gamma\left[V_0(t)\delta\gamma_0 + \delta K_0\int_{-\infty}^{t} dt'\ V_0(t')\right]\theta(t)e^{-\Gamma t} + \left[V_0(t)\ \delta\gamma_0 + \delta K_0\int_{-\infty}^{t} dt'\ V_0(t')\right]\delta(t). \tag{18}$$

In this paper, we only consider lifetimes much longer than the period of the driving field. Hence the second term may be neglected with respect to the first one. With this approximation the Fourier transform of the source term reads

$$-\tilde{S}(q) = \int_0^{\infty} dt[\dot{V}_0(t)\delta\gamma_0 + V_0(t)\delta K_0]e^{-(\Gamma+iq)t} + \left[V_0(0)\delta\gamma_0 + \delta K_0\int_{-\infty}^{0} dt' V_0(t')\right]. \tag{19}$$

It may be reduced to a single term using partial integration

$$-\tilde{S}(q) = (\Gamma + iq)\int_0^{\infty} dt \times \left[V_0(t)\delta\gamma_0 + \delta K_0\int_{-\infty}^{t} dt'\ V_0(t')\right]e^{-(\Gamma+iq)t}. \tag{20}$$

We now assume that the current source has been switched on in the infinite past, smoothly enough, for all transients to have disappeared at finite past times. The solution of Eq. (3) for the steady-state voltage is modified in the infinite past, $V_0(t \to -\infty) = 0$, without changing its form at finite times. The integral over the variable t' in Eq. (20) can then be done,

yielding

$$\tilde{S}(q) = \frac{I_0}{2C_0}(\Gamma + iq)[\delta K_0 + i\omega\delta\gamma_0]\frac{\tilde{G}(\omega)}{q - i\Gamma - \omega} - \{\bar{\omega}\}. \tag{21}$$

The symbol $-\{\bar{\omega}\}$ stands for a negative repeat of the first term with replacement of the positive frequency argument by a negative one. From Eq. (21) one may verify the reality property of the source term, which in Fourier domain implies $\tilde{S}^*(q) = \tilde{S}(-q^*)$. The Green function $\tilde{G}(q)$ also satisfies this property, whence the differential voltage $\tilde{u}(q)$, too (as a consequence of Eq. (15)).

V. CLOSED EXPRESSION FOR THE CYCLE-AVERAGED POWER

In the case of time-varying RLC values the cycle-averaged dissipated power varies with time, too, unlike in the time-independent case given in Eq. (6). The differential cycle-averaged power $\Delta\bar{P}^{\mathrm{diss}}(t_n)$ is defined at discrete time intervals t_n, with n an integer number

$$\bar{P}_0^{\mathrm{diss}} + \Delta\bar{P}^{\mathrm{diss}}(t_n) \equiv \frac{1}{T}\int_{t_n - T/2}^{t_n + T/2} dt' V(t') I_{RLC}(t')$$
$$t_n = nT = n\frac{2\pi}{\omega}. \tag{22}$$

Assuming small changes of the circuit parameters the differential cycle-averaged power can again be approximated by neglecting terms with a product of two differential quantities,

$$\Delta\bar{P}^{\mathrm{diss}}(t_n) = \frac{1}{T}\int_{t_n - T/2}^{t_n + T/2} dt' u(t')\left[I_0 \sin(\omega t') - \frac{2}{R_S}V_0(t')\right]. \tag{23}$$

This equation differs not only in the appearance of the differential quantity $u(t')$ instead of $V_0(t')$, but also in a factor 2 with respect to the steady-state expression (6). For the above treated case of a mono-exponential decay at rate Γ of the circuit parameters the integration over time (Eq. (23)) can be performed analytically. Using Eqs. (3), (4), (15) and (21), one obtains the following expression for the differential average dissipated power:

$$\Delta\bar{P}^{\mathrm{diss}}(t_n) = -\frac{I_0^2}{2\pi C_0 T} \times \mathrm{Re}\left\{\psi\tilde{G}(\omega)\int dq\, \frac{\tilde{G}(q)}{q - i\Gamma - \omega} f(q) e^{iqt_n}\right\}, \tag{24}$$

where use has been made of the definitions

$$f(q) \equiv (q - i\Gamma)(i\omega A + qB)\frac{e^{i\pi q/\omega} - e^{-i\pi q/\omega}}{q^2 - \omega^2}$$
$$\psi \equiv \delta K_0 + i\omega\delta\gamma_0$$
$$A \equiv 1 - 2\omega^2\gamma_S(\gamma_0 + \gamma_S)|\tilde{G}(\omega)|^2$$
$$B \equiv -2\omega\gamma_S(K_0 - \omega^2)|\tilde{G}(\omega)|^2 \tag{25}$$

In spite of the appearances, the function $f(q)$ in Eq. (25) has no poles, because the numerator's zeros exactly overlap with denominator's (at $q = \pm\omega$). Hence the integral in Eq. (24) can be written as a sum of only two terms, corresponding to the pole couples $q = \pm\omega + i\Gamma$ (due to the denominator in Eq. (24)) and $q = \pm\Omega + i\bar{\gamma}$ (due to the Green's function in Eq. (24), cf. Eqs. (4) and (5)),

$$\Delta\bar{P}^{\mathrm{diss}}(t_n) = \Delta\bar{P}_1^{\mathrm{diss}}(t_n) + \Delta\bar{P}_2^{\mathrm{diss}}(t_n)$$
$$\Delta\bar{P}_1^{\mathrm{diss}}(t_n) = \frac{I_0^2\omega}{2\pi C_0}\theta(t_n)e^{-\Gamma t_n} \times \mathrm{Im}[\psi\tilde{G}(\omega)\tilde{G}(\omega + i\Gamma)f(\omega + i\Gamma)]$$
$$\Delta\bar{P}_2^{\mathrm{diss}}(t_n) = \frac{I_0^2\omega}{2\pi C_0}\theta(t_n)e^{-\bar{\gamma}t_n} \times \mathrm{Im}\left[e^{i\Omega t_n}\psi\tilde{G}(\omega)\frac{-1/2\Omega}{\Omega + i\bar{\gamma} - i\Gamma - \omega} \times f(\Omega + i\bar{\gamma}) + \{\bar{\Omega}\}\right]. \tag{26}$$

The terms $\Delta\bar{P}_1^{\mathrm{diss}}(t_n)$ and $\Delta\bar{P}_2^{\mathrm{diss}}(t_n)$ in Eq. (26) correspond to the steady-state solution and the transient, respectively. The steady-state solution $\Delta\bar{P}_1^{\mathrm{diss}}(t_n)$ is not oscillatory, because the exponential $e^{i\omega t_n}$ in the residue of Eq. (24) equals unity for all times t_n (cf. Eq. (22)). The steady-state solution decays exponentially with the population decay rate of the charge carriers, Γ. The transient term $\Delta\bar{P}_2^{\mathrm{diss}}(t_n)$ decays with a rate $\bar{\gamma}$ determined by the width of the resonance, and oscillates at the difference frequency $\Omega - \omega$. This can be seen from the fact that the exponential functions $e^{i\Omega t_n}$ (discrete time variable) and $e^{i(\Omega-\omega)t}$ (continuous time variable) both have a repetition period $2\pi/|\Omega - \omega|$. It is a typical example of what is called *aliasing:* the frequency Ω is probed with another frequency ω, resulting in a temporally discretized signal displaying the difference frequency $\Omega - \omega$. The lowest frequency solution fitting the discretized signal is given by the following expressions:

$$\Delta\bar{P}_1^{\mathrm{diss}}(t) = \frac{4}{\pi}P_{AV}\omega\gamma_S\theta(t)e^{-\Gamma t} \times \mathrm{Im}[\psi\tilde{G}(\omega)\,\tilde{G}(\omega + i\Gamma)f(\omega + i\Gamma)]$$
$$\Delta\bar{P}_2^{\mathrm{diss}}(t) = \frac{4}{\pi}P_{AV}\omega\gamma_S\theta(t)e^{-\bar{\gamma}t} \times \mathrm{Im}\left[e^{i(\Omega-\omega)t}\frac{\psi\tilde{G}(\omega)}{2\Omega}\frac{f(\Omega + i\bar{\gamma})}{\omega - \Omega + i(\Gamma - \bar{\gamma})} + \{\bar{\Omega}\}\right]. \tag{27}$$

For resonance cavities with a high quality factor the oscillatory behavior of $\Delta\bar{P}_2^{\mathrm{diss}}(t)$ shows up in the time traces recorded on both sides of the resonance frequency ($|\omega - \Omega| \geq \gamma$), while disappearing at resonance ($\omega \approx \Omega \approx \sqrt{K_0}$). The oscillatory behavior modulates the rise time as a function of driving frequency: the closer to resonance, the longer the rise time. This is in agreement with the physical picture that the electromagnetic field is longer lived at resonance; i.e., more

round trips of the field are needed at resonance to reach a new equilibrium.

The transient solution $\Delta\bar{P}_2^{\text{diss}}(t)$ embodies the radical difference in short-time response of the cavity to changes in $\delta\gamma_0$ and δK_0. A change in δK_0 implies a change in the resonance frequency of the cavity. This change is experienced fully and immediately by the electric field in the resonance cavity, i.e., after only a single round trip. On the other hand, a change in $\delta\gamma_0$ is only experienced by the electric field after a number of round trips, equal to the quality factor of the resonance cavity.

In the limit of infinite lifetime ($\Gamma = 0$) the $\Delta\bar{P}_1^{\text{diss}}(t)$ term in Eq. (27) reduces to the steady-state response of the cavity, as can be ascertained on comparing Eqs. (6) and (27). From Eq. (6) the differential power absorption can be calculated by taking partial derivatives to the circuit parameter γ_0 and K_0,

$$\frac{\partial\bar{P}_0^{\text{diss}}}{\partial\gamma_0} = 4\omega^2\gamma_S P_{AV}\left\{1+\gamma_0\frac{\partial}{\partial\gamma_0}\right\}|\tilde{G}(\omega)|^2 = 4\omega^2\gamma_S P_{AV}\left\{(K_0-\omega^2)^2+\omega^2\left(\gamma_S^2-\gamma_0^2\right)\right\}|\tilde{G}(\omega)|^4, \tag{28}$$

$$\frac{\partial\bar{P}_0^{\text{diss}}}{\partial K_0} = -8\omega^2\gamma_0\gamma_S P_{AV}(K_0-\omega^2)|\tilde{G}(\omega)|^4. \tag{29}$$

On the other hand, from Eq. (26) one has for $\Gamma = 0$,

$$\Delta\bar{P}_1^{\text{diss}}(t)\big|_{\Gamma=0} = \frac{4}{\pi}P_{AV}\omega\gamma_S\theta(t)\text{Im}[\psi\tilde{G}^2(\omega)f(\omega)] = 4P_{AV}\omega\gamma_S\theta(t)\text{Im}[\psi\tilde{G}^2(\omega)(A-iB)], \tag{30}$$

where use has been made of Eqs. (28) and (29), and of the limiting expression $f(\omega)|_{\Gamma=0} = \pi(A - iB)$, which follows directly from the definition (25). From Eq. (28) through Eq. (30) one may obtain the following identity:

$$\Delta\bar{P}_1^{\text{diss}}(t)\big|_{\substack{\Gamma=0\\ \delta\chi_0=0}} = \frac{\partial\bar{P}_0^{\text{diss}}}{\partial K_0}\delta K_0 + \frac{\partial\bar{P}_0^{\text{diss}}}{\partial\gamma_0}\delta\gamma_0, \tag{31}$$

thus confirming the term $\Delta\bar{P}_1^{\text{diss}}(t)$ in Eq. (27).

VI. COMPARISON WITH EXPERIMENTAL RESULTS

In order to illustrate the cavity response described by Eq. (27) we now proceed to comparing the calculated response with experimental data obtained by means of an experimental technique called TRMC.[3–13]

In this technique a waveguide is terminated by a resonant cavity. The unloaded cavity has a quality factor $Q_{\text{unloaded}} = 500$. We use a resonance frequency in the X-band of $\omega_{\text{res}}/2\pi = 9$ GHz, hence $\gamma_S/2\pi = 18$ MHz. The loaded cavity has a slightly lower quality factor, usually around $Q_{\text{loaded}} = 400$, implying $\gamma_0/2\pi = 4.5$ MHz. Using Eq. (8), the fraction of reflected power at resonance then amounts to $\bar{P}_0^{\text{refl}}/P_{AV} = 60\%$.

The loaded cavity contains the sample with unknown conductivity and dielectric constant. The sample's conductivity and dielectric constant can be deduced by measuring the microwave power reflected from the cavity, $\bar{P}_0^{\text{refl}} = P_{AV} - \bar{P}_0^{\text{diss}}$, with and without sample in the cavity: the sample's conductivity causes a reduction in the reflected power, and the sample's dielectric constant causes a shift of the resonance frequency. The sample's conductivity and dielectric constant are linearly related to the steady-state circuit parameters, γ_0 and K_0, respectively. The relation between these circuit parameters and the sample dielectric properties are given in Appendix B.

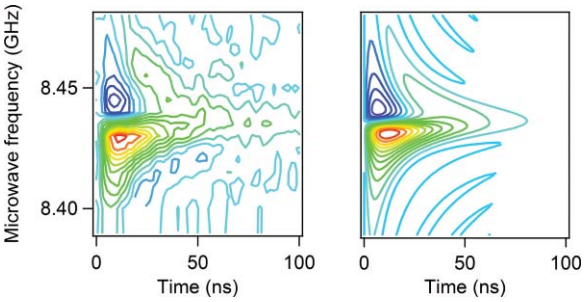

FIG. 2. (Color online) (left) Measured microwave spectrum (film of CdSe nanocrystals on a quartz substrate). (Right) Model calculation of the quantity $\Delta\bar{P}^{\text{diss}}(t)/\bar{P}_0^{\text{refl}}$ using Eqs. (27) and (6). Two species are involved. The longer lived ($\Gamma^{-1} = 30$ ns) species has a mixed signature with $\delta K_0 = 2\omega_{\text{res}}\delta\gamma_0$. The shorter lived species ($\Gamma^{-1} = 10$ ns) is purely imaginary ($\delta\gamma_0 = 0$).

Once the sample's conductivity and dielectric constant have been established, its response to photo-excitation can be measured. The data are displayed in two dimensions, as a function of (continuous) time, and of (discrete) frequency, in the form of the ratio $\Delta\bar{P}^{\text{refl}}(t)/\bar{P}_0^{\text{refl}}$, the fractional change in reflected power. The two-dimensional data allow for extraction of the dynamic parameters, $\delta\gamma_0$ and δK_0. These two parameters can again be converted to photo-induced changes in the sample's conductivity and dielectric constant, respectively, using the expressions derived in Appendix B.

The samples were excited by a 3 ns pump pulse. Since the cavity rise time (18 ns) largely exceeds the duration of the pump pulse, there was no need to convolve the model calculations with the pump pulse.

A mixed signal containing both a real and an imaginary conductivity is presented in Fig. 2. The measurement corresponds to a thin film of CdSe nanocrystals (cf. Appendixes A and B for preparation details). For the calculation two species were used with lifetimes of 10 and 30 ns. The longer lived species is of mixed character with $\delta K_0 = 2\omega_{\text{res}}\delta\gamma_0$. The shorter lived species only carries imaginary conductivity: that is to say, the charge carriers are either excitons or quasi-free charges on a small, bounded domain.

A purely imaginary conductivity is displayed by a dilute solution of CdSe nanocrystals, as shown in Fig. 3 (left). This is consistent with the fact that only excitons are created by the pump pulse. These excitons are confined to the nanocrystal in which they were created. The calculations (Fig. 3, right) reproduce the main features shown in the measured data on assuming a single species with purely imaginary conductivity and 40 ns lifetime. Like in the previous case (cf. Fig. 2) the experimental data show the presence of a longer lived component, which we did not include in the calculations for didactical reasons. A serious fit generally requires several exponential decay times for every species.

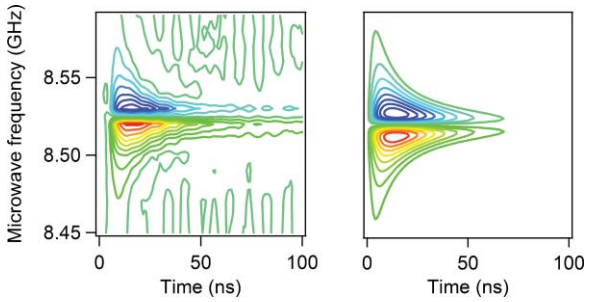

FIG. 3. (Color online) (left) Measured microwave spectrum for a dispersion of CdSe nanocrystals. (Right) Model calculation with $\delta\gamma_0 = 0$: there is no net dissipation and the signal is exclusively due to a change in polarizability ($\delta K_0 \neq 0$). The calculation was done with a single lifetime only: $\Gamma^{-1} = 40$ ns.

A predominantly real conductivity is displayed by the bulk crystal TiO_2, photo-excited above the bandgap, as shown in Fig. 4 (left). The slight asymmetry at long times (100 ns) betrays the presence of a long-lived imaginary component. The calculation was performed for a single species only, with a lifetime far exceeding the 100 ns window. This species is of mixed character with $\delta K_0 = \omega_{res}\delta\gamma_0$. As mentioned in Sec. V, one may appreciate that for times below the cavity rise time, the change in the dielectric constant (related to δK_0) dominates the signal, leading to a shift of the resonance frequency. At times exceeding the cavity rise time, the change in the conductivity (related to $\delta\gamma_0$) dominates the signal, leading to increased dissipation. The mixed character of the species results in a sign change of the signal for driving frequencies beyond the resonance frequency, while the signal keeps positive throughout for driving frequencies below the resonance frequency. The negative lobe at high driving frequency lasts very short, corresponding to the cavity rise time. The similarity of the calculations with the experimental data can be improved (this was again not done for didactical reasons) upon adding a second species to the signal, of purely imaginary character, with a slow rate of ingrowth. Such a species does not affect the initial (below the cavity rise time) two-dimensional pattern, while contributing to the asymmetry of the pattern at long times (100 ns).

The above comparison of our model calculations with selected experimental data shows that Eq. (27) is able to provide a quantitative account of all the experimentally observed features. The model is useful for absorptive signals that are too weak to be measurable with an "open cell" (i.e., short circuited waveguide with unit quality factor). A resonance cell is necessary for measuring changes in the dielectric constant. A particularly interesting insight arising from the present model, is the following: for a single photo-excited species displaying a change in both conductivity and dielectric constant, the two-dimensional spectra show a transition from a predominantly dielectric (on short times) to a predominantly absorptive (at long times compared to the cavity rise time) characteristic (cf. the calculation for TiO_2 in Fig. 4). This is due to the fact that the absorptive response sets in slowly, on the time scale of the cavity rise time, while the dielectric response (the shift in resonance frequency) occurs instantaneously (after a single cavity round trip time of the microwave field). Though simple to grasp once realized, this effect has led to misinterpretations in the past: a spectrum like that in Fig. 4 would readily be interpreted as due to a short-lived excitonic component, and a longer-lived free charge, while in fact the two components have the same lifetime; worse, the data indicate the presence of a slowly growing, purely imaginary contribution.

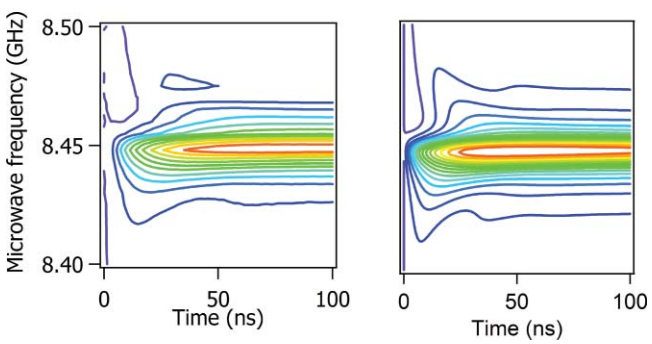

FIG. 4. (Color online) (left) Measured microwave spectrum (TiO_2 film on a quartz substrate). (Right pane) Model calculation for a predominantly real conductivity. Parameters used for the model calculation: $\delta K_0 = \omega_{res}\delta\gamma_0$, lifetime 1000 ns.

We have presented a quantitative description of the transient behavior of semiconductors in a resonant cavity probed by microwave radiation. The price to pay for the resonant cavity is the long response time, but the advantages are a drastic improvement of the signal-to-noise ratio and the capability to distinguish dissipative from dielectric effects.

ACKNOWLEDGMENTS

We are grateful to Tom Savenije for pointing out to us the lack of a time-dependent description of Time-Resolved Microwave Conductivity.

APPENDIX A: SAMPLE PREPARATION

All experiments were carried under N_2 atmosphere and anhydrous solvents were used.

Film of CdSe *nanocrystals* (Fig. 2): CdSe nanocrystals with a 3 nm diameter were synthesized following the "green" recipe of Mekis *et al.*[63] This synthesis resulted in nanocrystals stabilized by a combination of tri-n-octylphosphine oxide (TOPO), hexadecylamine, and n-tetradecylphosphonic acid ligand molecules. The nanocrystals were precipitated with methanol, filtered and redispersed in toluene. After repeating the latter procedure twice, the nanocrystals were dispersed in a 9:1 v/v chloroform/octane mixture. Films were prepared by drop-casting the nanocrystal dispersion on a quartz plate.

CdSe *nanocrystal dispersion* (Fig. 3): CdSe nanocrystals with a 10 nm diameter were synthesized following the synthesis in stearic acid of Yu *et al.*[64] with some modifications. 8 g of TOPO were degassed in a Schlenk line at 180 °C. The solution was allowed to cool down to 130 °C and a dispersion of 0.276 g of $Cd(Ac)_2$ in 16 g of oleic acid (OA) was added to the TOPO. The mixture was kept at 130 °C until it became optically clear due to the formation of $Cd(OA)_2$. Next, the mixture was brought to 340 °C and a solution composed of 0.316 g of

Se in 12 mL of TOP was quickly injected under vigorous stirring, resulting in the formation of CdSe nanocrystals. Growth of the nanocrystals was carried out at 300 °C for 5 min. After cooling of the dispersion, the nanocrystals were precipitated with methanol, filtered and redispersed in toluene. The latter procedure was repeated twice and the nanocrystals were dispersed in hexane.

TiO_2 *film* (Fig. 4): 100 nm-thick anatase TiO_2 layers on quartz substrates were produced by Everest Coating, Delft, The Netherlands.

APPENDIX B: RELATION BETWEEN THE SAMPLE'S DIELECTRIC CONSTANT AND THE LUMPED CIRCUIT PARAMETERS

In waveguide theory, the dimensionless complex relative admittance $Y(z,\omega)$ is defined as the ratio between the space (z) and frequency (ω) dependent magnetic ($H(z,\omega)$) and electric fields ($E(z,\omega)$) as follows:[65,66]

$$Y(z,\omega) \equiv \sqrt{\frac{\mu_0}{\varepsilon_0}} \frac{H(z,\omega)}{n(\omega)E(z,\omega)}, \tag{B1}$$

with $n(\omega)$ the index of refraction, and μ_0 and ε_0 the vacuum magnetic permeability and electric permittivity, respectively. The dimensionless complex reflection coefficient $\Gamma(z,\omega)$ is related to the relative admittance as

$$\Gamma(z,\omega) = \frac{1 - Y(z,\omega)}{1 + Y(z,\omega)}. \tag{B2}$$

For a resonant cavity with length d the ratio of reflected to incident power is given by the square modulus of the reflection coefficient,

$$\frac{\bar{P}_0^{\text{refl}}}{P_{AV}} = |\Gamma(d,\omega)|^2, \tag{B3}$$

with the relative admittance equal to

$$Y(d,\omega) = \coth(ikd) - iB, \tag{B4}$$

where B characterizes the leak loss of the iris, and $k = k' + ik''$ represents the complex wave number. The relation of the real part of the wave number to frequency is given by the dispersion relation in the waveguide

$$k' \equiv \sqrt{\left(\frac{\omega}{c}\right)^2 - \left(\frac{\pi}{a}\right)^2}, \qquad k_0 \equiv k'(\omega_{\text{res}}) \tag{B5}$$

where the term $(\pi/a)^2$ characterizes the lowest spatial mode in the waveguide of width a. The imaginary part of the wave number accounts for (i) heat loss of mode-sustaining currents in the cavity walls, and (ii) absorption of microwave radiation by the thin film under study,

$$k'' = k''_{\text{wall}} + k''_{\text{sample}}. \tag{B6}$$

Comparison of Eq. (B3) with Eq. (6) yields the following identities:

$$\Delta k'' = -\frac{\omega_{\text{res}}}{2c^2 k_0}\Delta\gamma_0, \tag{B7}$$

$$\Delta k' = \frac{\gamma_S}{2c^2 k_0(\gamma_0 + \gamma_S)}\Delta K_0. \tag{B8}$$

These identities apply in the case of high quality factors, i.e., assuming a Lorentzian profile of the dissipated power as a function of driving frequency.

In a standard measurement procedure one starts by recording the power dip $\bar{P}_0^{\text{refl}}(\omega)$, which determines the resonance frequency ω_{res} and the RLC parameters γ_0 and γ_S. Next, the photo-excited 2D spectra are taken, yielding the fit parameters $\Delta\gamma_0$ and ΔK_0 for every lifetime component Γ, by means of Eq. (27). Using Eqs. (B7) and (B8), these fit parameters can be transformed into changes in complex wave number $\Delta k'$, Δk. The changes in complex dielectric constant then follow from the relations

$$\begin{aligned}\Delta\varepsilon'_s &= 2\left(\frac{c}{\omega}\right)^2 (k'\Delta k' - k''\Delta k''),\\ \Delta\varepsilon''_s &= 2\left(\frac{c}{\omega}\right)^2 (k'\Delta k'' + k''\Delta k').\end{aligned} \tag{B9}$$

Equation (B9) applies for a gaseous sample, homogeneously filling the cavity. In the case of thin film samples these expressions should be adapted to account for film thickness and dielectric constant.

[1] H. Margenau, Phys. Rev. **69**, 508 (1946).
[2] H. Margenau, F. L. McMillan, I. H. Dearnley, C. S. Pearsall, and C. G. Montgomery, Phys. Rev. **70**, 349 (1946).
[3] M. A. Biondi and S. C. Brown, Phys. Rev. **75**, 1700 (1949).
[4] M. A. Biondi and S. C. Brown, Phys. Rev. **76**, 1697 (1949).
[5] S. C. Brown and D. J. Rose, J. Appl. Phys. **23**, 711 (1952).
[6] D. J. Rose and S. C. Brown, J. Appl. Phys. **23**, 719 (1952).
[7] D. J. Rose and S. C. Brown, J. Appl. Phys. **23**, 1028 (1952).
[8] R. W. Fessenden and J. M. Warman, Adv. Chem. Ser. **82**, 222 (1968).
[9] J. M. Warman and R. W. Fessenden, J. Chem. Phys. **49**, 4718 (1968).
[10] J. M. Warman and M. C. Sauer, J. Chem. Phys. **52**, 6428 (1970).
[11] A. F. Gibson, Proc. Phys. Soc. London, Sect. B **69**, 488 (1956).
[12] A. F. Gibson, J. W. Granville, and E. G. S. Paige, J. Phys. Chem. Solids **19**, 198 (1961).
[13] J. A. Naber and D. P. Snowden, Rev. Sci. Instrum. **40**, 1137 (1969).
[14] J. M. Warman, M. P. Dehaas, and A. Hummel, Chem. Phys. Lett. **22**, 480 (1973).
[15] J. B. Verberne, H. Loman, J. M. Warman, M. P. Dehaas, A. Hummel, and L. Prinsen, Nature (London) **272**, 343 (1978).
[16] M. Kunst and J. M. Warman, Nature (London) **288**, 465 (1980).
[17] D. Vanlith, M. P. Dehaas, J. M. Warman, and A. Hummel, Biopolymers **22**, 807 (1983).
[18] D. Vanlith, J. Eden, J. M. Warman, and A. Hummel, J. Chem. Soc., Faraday Trans. 1 **82**, 2945 (1986).
[19] D. Vanlith, J. M. Warman, M. P. Dehaas, and A. Hummel, J. Chem. Soc., Faraday Trans. 1 **82**, 2933 (1986).
[20] R. Hoofman, G. P. vanderLaan, M. P. deHaas, and K. Tanigaki, Synth. Met. **86**, 2355 (1997).
[21] J. M. Warman and A. M. Van de Craats, Mol. Cryst. Liq. Cryst. **396**, 41 (2003).
[22] J. M. Warman, G. H. Gelinck, and M. P. de Haas, J. Phys. Condens. Matter **14**, 9935 (2002).
[23] M. P. Dehaas and J. M. Warman, Chem. Phys. **73**, 35 (1982).
[24] R. W. Fessenden, P. M. Carton, H. Shimamori, and J. C. Scalano, J. Phys. Chem. **86**, 3803 (1982).
[25] F. Wunsch, D. Klein, A. Podlasly, A. Ostmann, M. Schmidt, and M. Kunst, Sol. Energy Mater. Sol. Cells **93**, 1024 (2009).
[26] T. Mayer, U. Weiler, C. Kelting, D. Schlettwein, S. Makarov, D. Wohrle, O. Abdallah, M. Kunst, and W. Jaegermann, Sol. Energy Mater. Sol. Cells **91**, 1873 (2007).
[27] S. von Aichberger, H. Feist, J. Loffler, and M. Kunst, Sol. Energy Mater. Sol. Cells **65**, 417 (2001).
[28] A. Sanders and M. Kunst, Solid-State Electron. **34**, 1007 (1991).

[29]A. Meeder, D. F. Marron, M. C. Lux-Steiner, and M. Kunst, Compound Semiconductor Photovoltaics Book Series, Mater. Res. Soc. Symp. Proc. **763**, 41 (2003).
[30]T. Weiss, M. Birkholz, M. Saad, S. Bleyhl, M. Kunst, A. Jager-Waldau, and M. C. Lux-Steiner, J. Cryst. Growth **198**, 1190 (1999).
[31]A. M. vandeCraats, J. M. Warman, M. P. deHaas, D. Adam, J. Simmerer, D. Haarer, and P. Schuhmacher, Adv. Mater. **8**, 823 (1996).
[32]A. M. van de Craats, L. D. A. Siebbeles, I. Bleyl, D. Haarer, Y. A. Berlin, A. A. Zharikov, and J. M. Warman, J. Phys. Chem. B **102**, 9625 (1998).
[33]Z. S. An, J. S. Yu, S. C. Jones, S. Barlow, S. Yoo, B. Domercq, P. Prins, L. D. A. Siebbeles, B. Kippelen, and S. R. Marder, Adv. Mater. **17**, 2580 (2005).
[34]P. Prins, K. Senthilkumar, F. C. Grozema, P. Jonkheijm, A. P. H. J. Schenning, E. W. Meijer, and L. D. A. Siebbeles, J. Phys. Chem. B **109**, 18267 (2005).
[35]A. Zen, P. Pingel, F. Jaiser, D. Neher, J. Grenzer, W. Zhuang, J. P. Rabe, A. Bilge, F. Galbrecht, B. S. Nehls, T. Farrell, U. Scherf, R. D. Abellon, F. C. Grozema, and L. D. A. Siebbeles, Chem. Mater. **19**, 1267 (2007).
[36]P. Pingel, A. Zen, R. D. Abellon, F. C. Grozema, L. D. A. Siebbeles, and D. Neher, Adv. Funct. Mater. **20**, 2286 (2010).
[37]W. J. Grzegorczyk, T. J. Savenije, J. J. P. Valeton, S. Fratiloiu, F. C. Grozema, D. M. de Leeuw, and L. D. A. Siebbeles, J. Phys. Chem. C **111**, 18411 (2007).
[38]A. Demenev, S. H. Eichhorn, T. Taerum, D. F. Perepichka, S. Patwardhan, F. C. Grozema, L. D. A. Siebbeles, and R. Klenkler, Chem. Mater. **22**, 1420 (2010).
[39]I. Paraschiv, K. de Lange, M. Giesbers, B. van Lagen, F. C. Grozema, R. D. Abellon, L. D. A. Siebbeles, E. J. R. Sudholter, H. Zuilhof, and A. T. M. Marcelis, J. Mater. Chem. **18**, 5475 (2008).
[40]F. C. Grozema, T. J. Savenije, M. J. W. Vermeulen, L. D. A. Siebbeles, J. M. Warman, A. Meisel, D. Neher, H. G. Nothofer, and U. Scherf, Adv. Mater. **13**, 1627 (2001).
[41]B. R. Wegewijs, L. D. A. Siebbeles, N. Boden, R. J. Bushby, B. Movaghar, O. R. Lozman, Q. Liu, A. Pecchia, and L. A. Mason, Phys. Rev. B **65** (2002).
[42]P. A. C. Quist, J. Sweelssen, M. M. Koetse, T. J. Savenije, and L. D. A. Siebbeles, J. Phys. Chem. C **111**, 4452 (2007).
[43]P. A. C. Quist, T. J. Savenije, M. M. Koetse, S. C. Veenstra, J. M. Kroon, and L. D. A. Siebbeles, Adv. Funct. Mater. **15**, 469 (2005).
[44]P. Prins, F. C. Grozema, J. M. Schins, T. J. Savenije, S. Patil, U. Scherf, and L. D. A. Siebbeles, Phys. Rev. B **73**, 045204 (2006).
[45]X. Q. Li, V. Stepanenko, Z. J. Chen, P. Prins, L. D. A. Siebbeles, and F. Wurthner, Chem. Commun. (Cambridge) **37**, 3871 (2006).
[46]W. J. Grzegorczyk, T. J. Savenije, T. E. Dykstra, J. Piris, J. M. Schins, and L. D. A. Siebbeles, J. Phys. Chem. C **114**, 5182 (2010).
[47]W. J. Grzegorczyk, T. J. Savenije, M. Heeney, S. Tierney, I. McCulloch, S. van Bavel, and L. D. A. Siebbeles, J. Phys. Chem. C **112**, 15973 (2008).
[48]P. Prins, F. C. Grozema, and L. D. A. Siebbeles, J. Phys. Chem. B **110**, 14659 (2006).
[49]A. A. Kocherzhenko, S. Patwardhan, F. C. Grozema, H. L. Anderson, and L. D. A. Siebbeles, J. Am. Chem. Soc. **131**, 5522 (2009).
[50]F. C. Grozema, C. Houarner-Rassin, P. Prins, L. D. A. Siebbeles, and H. L. Anderson, J. Am. Chem. Soc. **129**, 13370 (2007).
[51]P. Prins, F. C. Grozema, J. M. Schins, S. Patil, U. Scherf, and L. D. A. Siebbeles, Phys. Rev. Lett. **96**, 146601 (2006).
[52]F. C. Grozema, L. D. A. Siebbeles, J. M. Warman, S. Seki, S. Tagawa, and U. Scherf, Adv. Mater. **14**, 228 (2002).
[53]R. Katoh, A. Furube, K. Yamanaka, and T. Morikawa, J. Phys. Chem. Lett. **1**, 3261 (2010).
[54]R. Katoh, A. Huijser, K. Hara, T. J. Savenije, and L. D. A. Siebbeles, J. Phys. Chem. C **111**, 10741 (2007).
[55]R. Katoh, M. Kasuya, A. Furube, N. Fuke, N. Koide, and L. Y. Han, Sol. Energy Mater. Sol. Cells **93**, 698 (2009).
[56]J. Piris, A. J. Ferguson, J. L. Blackburn, A. G. Norman, G. Rumbles, D. C. Selmarten, and N. Kopidakis, J. Phys. Chem. C **112**, 7742 (2008).
[57]J. Piris, N. Kopidakis, D. C. Olson, S. E. Shaheen, D. S. Ginley, and G. Rumbles, Adv. Funct. Mater. **17**, 3849 (2007).
[58]A. J. Ferguson, N. Kopidakis, S. E. Shaheen, and G. Rumbles, J. Phys. Chem. C **112**, 9865 (2008).
[59]T. Moehl, V. G. Kytin, J. Bisquert, M. Kunst, H. J. Bolink, and G. Garcia-Belmonte, ChemSusChem **2**, 314 (2009).
[60]J. J. Piet, P. N. Taylor, B. R. Wegewijs, H. L. Anderson, A. Osuka, and J. M. Warman, J. Phys. Chem. B **105**, 97 (2001).
[61]J. J. Piet, P. N. Taylor, H. L. Anderson, A. Osuka, and J. M. Warman, J. Am. Chem. Soc. **122**, 1749 (2000).
[62]G. H. Gelinck, J. J. Piet, B. R. Wegewijs, K. Mullen, J. Wildeman, G. Hadziioannou, and J. M. Warman, Phys. Rev. B **62**, 1489 (2000).
[63]I. Mekis, D. V. Talapin, A. Kornowski, M. Haase, and H. Weller, J. Phys. Chem. B **107**, 7454 (2003).
[64]L. H. Qu, Z. A. Peng, and X. G. Peng, Nano Lett. **1**, 333 (2001).
[65]J. M. Schins, P. Prins, F. C. Grozema, R. D. Abellon, M. P. de Haas, and L. D. A. Siebbeles, Rev. Sci. Instrum. **76**, 084703 (2005).
[66]P. P. Infelta, M. P. D. Haas, and J. M. Warman, Radiat. Phys. Chem. **10**, 353 (1977).